Nuclear and Emerging Technologies for Space, American Nuclear Society Topical Meeting
Richland, WA, February 25 – February 28, 2019, available online at http://anstd.ans.org/

DESIGN AND ANALYSIS OF A NpO_2 TARGET FOR THE PRODUCTION OF ^{238}Pu

Joel L. McDuffee[1], Padhraic L. Mulligan[1], Kurt R. Smith[1], and Robert M. Wham[1]

[1]*Oak Ridge National Laboratory, 1 Bethel Valley Road, Oak Ridge, TN, 37831, 865-241-0873, mcduffeej@ornl.gov*

Current production of ^{238}Pu at Oak Ridge National Laboratory uses NpO_2–aluminum cermet pellets as the feed material. The advantage of cermet is that its thermal conductivity is much higher than that of the oxide alone, which greatly reduces pellet temperatures. However, the melting point of the material is quite low due to the aluminum in the matrix, and the recovery of the ^{238}Pu results in substantial radioactive liquid waste. There is potentially both a significant production gain and a reduction in post-irradiation processing cost and waste associated with using a pure NpO_2 pellet. This work describes ongoing efforts to design a NpO_2 pellet to maximize production of ^{238}Pu in the High Flux Isotope Reactor.

I. INTRODUCTION

NpO_2–aluminum cermet production targets have been used in the production of ^{238}Pu from the beginning of the technology. The Savannah River Site was the first to make ^{238}Pu on a production scale, and they developed much of the technology associated with the cermet target design (Ref. 1).

There are advantages to using a cermet target. The higher thermal conductivity keeps irradiation temperatures lower, which also improves dissolution, and the aluminum can be removed chemically. However, the cermet form also has significant costs associated with it. The higher thermal conductivity also comes with reduced temperature margins. The melting points of aluminum and NpO_2 are 660°C and 2800°C, respectively, and the lower melting point limits production by restricting the mass of ^{237}Np feedstock that can be loaded into each pellet. The ease of chemically removing the aluminum is belied by the disposal cost of radioactive liquid waste.

Pure NpO_2 targets have the potential to both improve production and reduce the waste stream associated with harvesting the ^{238}Pu from irradiated targets. However, the low thermal conductivity of NpO_2 and high heat generation make the target qualification difficult. This study summarizes ongoing efforts to design and qualify a pure NpO_2 target for irradiation in the High Flux Isotope Reactor (HFIR) at Oak Ridge National Laboratory (ORNL) and in the Advanced Test Reactor (ATR) at Idaho National Laboratory.

II. PHASE I DESIGN AND IRRADIATION

No documented irradiation studies have used pure NpO_2 pellets. Therefore, the design incorporates several conservative design features into the Phase I target design. As testing progresses into Phase II, this conservatism will be scaled back as measured data accumulates.

II.A Phase I Target Design

The NpO_2 rodlet assembly consists of a zircaloy-4 cladding enclosing four NpO_2 pellets whose diameters match that of a common UO_2 light water reactor fuel. The pellet stack is sandwiched between two hafnia pellets of similar diameter. The pellet stack is supported from the bottom by a molybdenum spacer tube and a stainless steel compression spring on the top. Ir-40Pt melt wires were placed inside a blind hole in the NpO_2 pellets and will be used for temperature verification. Fig. 1 shows the assembled rodlet. A small radial gas gap is imposed between the NpO_2 pellets and zircaloy cladding to ensure proper heat transfer between parts and minimize stress to the cladding as the pellet swells.

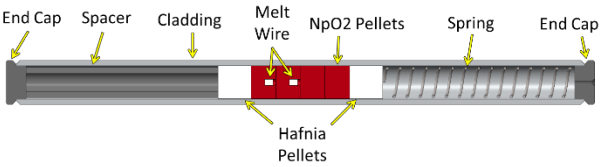

Fig. 1. NpO_2 qualification rodlet assembly.

As shown in Fig. 2, each rodlet assembly is placed inside a larger capsule assembly, which serves as a secondary containment vessel. This capsule consists of an aluminum 6061-T6 housing tube and end caps. A molybdenum spacer tube is placed in the bottom to support the rodlet assembly, and a stainless steel compression spring is located in the upper plenum. A hafnium disk sits between the top compression spring and the rodlet to act as an axial neutron shield.

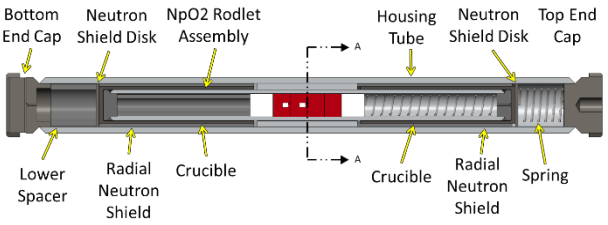

Fig. 2. NpO_2 qualification capsule assembly.

Surrounding the outer diameter of the rodlet assembly, on the top and bottom portions, is a hafnium neutron shield and tungsten crucible, as shown in Fig. 2. The purpose of the crucible is to contain NpO_2 material in the event melting occurs. The hafnium surrounding the crucible is designed to shield the melt from thermal neutrons, greatly reducing the fission heat rate and allowing the material to re-solidify.

The Phase I target only includes a single, four-pellet stack in each irradiation facility to minimize the material at risk. However, this introduces a difference with respect to a fully loaded target array. The other targets in the production array effectively shield each other from the surrounding neutron field. To compensate for this effect, the region surrounding the midsection of the rodlet is 180 degrees of the aluminum housing and a 175 degree hafnium shield, as shown in Fig. 3. This hafnium shield simulates the effect of neutron absorption in other pellets that will be present in the larger production assembly.

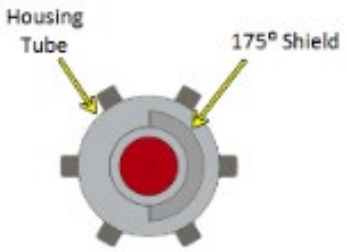

Fig. 3. Phase I target cross-section showing partial shield.

II.B. NpO_2 Neutronics and Depletion Modeling

Determining heat generation rates and expected ^{238}Pu yield is essential to performing safety and feasibility analyses for the phase I capsule design. A neutronics model of the HFIR cycle 400 core (Ref. 2) was modified in MCNP5 (Ref. 3) to include the phase I capsule in an SVXF position. To accelerate solution convergence, the ADVANTG 3.0.3 code (Ref. 4) was used to calculate spatial and energy weight windows, as well as source bias cards, for each day of the assumed 26 day HFIR cycle. Additionally, time-dependent fission source distributions, fuel element burnup, and control element burnup values were calculated over the course of a HFIR cycle using VESTA 2.0.2 (Ref. 5) and tabulated for use during core simulations. Using these precalculated values and historical control plate positions avoided having to perform lengthy k-code simulations and time-dependent material depletion calculations for each timestep of the HFIR cycle.

Pellets were modeled individually by sectioning each into 10 radial and 8 azimuthal segments of equal volume for a total of 80 subsections per pellet. A total of 113 isotopes consisting of actinides, fission products, and light elements were tracked in each pellet subsection. The self-shielded absorption and fission, where applicable, ENDF/B-VII.1 (Ref. 6) cross sections were calculated for each isotope in each subsection, along with the 239-group energy-dependent neutron flux. Tallies for heat generation rates due to prompt fission and gammas were also tracked for each subsection.

Isotope depletion in the NpO_2 pellets was determined using the ORIGEN-S code in SCALE 6.1. A custom python script was created to collect self-shielded cross sections and flux spectra from MCNP output files for reformatting as input files for ORIGEN. Isotopes were then depleted using a 1 to 5 day timestep and reused as new pellet subsection material cards in MCNP simulations. Local decay heat due to alpha and beta emission was also determined in the ORIGEN simulations, as well as gamma spectra to be used in follow-on radiation transport modeling. A total of 40 depletion/neutron transport iterations were completed to simulate four cycles of irradiation. Once completed, the results provided time-dependent, total heat generation rates as a function of radial and azimuthal position in each pellet, along with local burnup, fission gas production, and ^{238}Pu yield.

Heat generation rates in the pellets were greatest in the outermost radial subsections and peaked in the azimuthal section facing the HFIR fuel. As Fig. 4 shows, the pellet subsection nearest the HFIR core generates 640 W/g on the last day of the fourth cycle, while only 4 mm away in the pellet center, the heat generation peaks at 52 W/g. These heat generation rates were then used as inputs for thermal models, along with burnup values calculated to modify burnup-dependent thermophysical properties.

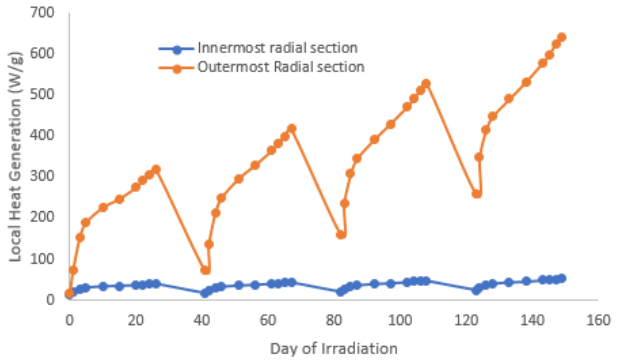

Fig. 4. Heat generation rates calculated in two radial subsections of an NpO_2 pellet irradiated over four HFIR cycles.

II.C. NpO_2 Thermophysical Properties

While the unirradiated thermophysical properties of NpO_2 are generally known, how burnup and radiation affect those properties is not well understood. This is unfortunate since the thermal conductivity of the pellet has a large influence on the estimated temperature. However, the behavior of UO_2, which is a closely related actinide oxide, has been well studied. Therefore, a set of material properties is developed that makes best use of measured, unirradiated NpO_2 properties while assuming that irradiated behavior is similar to that of UO_2.

Experimental thermal conductivity measurements on NpO_2 were performed by Nishi et al. (Ref. 7) over the temperature range 300°C to 1200°C. An expression correlating thermal conductivity in NpO_2 pellets of 96% theoretical density (TD) to temperature was given as

$$k(T)_{96} = \frac{1}{0.09447 + 1.797 \times 10^{-4} T} \left(\frac{W}{m \cdot K}\right) \quad (1)$$

where T is temperature in Kelvin. This can be adjusted to any TD (Ref. 8):

$$k(T)_d = k(T)_{96} \left(\frac{1-p}{1+0.5p}\right)\left(\frac{1+0.5*0.04}{1-0.04}\right) \quad (2)$$

where p is the porosity of the material ($1 -$ theoretical density). Converting to 95% TD, this alters the coefficients of Eq. (1) to

$$k(T)_{95} = \frac{1}{0.09593 + 1.825 \times 10^{-4} T} \left(\frac{W}{m \cdot K}\right) \quad (3)$$

Reduction in the thermal conductivity of UO_2 due to irradiation effects (e.g., fission products in the crystal matrix, irradiation defects, annealing of irradiation defects) has been well characterized from experimental measurements on UO_2 samples with a range of burnup. The terms from the modified Nuclear Fuels Industries (NFI) model for UO_2 which account for burnup-induced changes to thermal conductivity are used in the model for thermal conductivity in NpO_2.

For UO_2, a model similar to Eq. (3) for thermal conductivity due to phonon scattering was modified to account for burnup effects in irradiated fuel. This model, named the modified NFI model (Ref. 9), is given as

$$k_{95}(T, Bu) = \frac{1}{A + BT + f(Bu) + (1 - 0.9e^{-0.04Bu}) g(Bu) h(T)} + \frac{E}{T^2} e^{-F/T} \quad (4)$$

where A and B are the coefficients for phonon scattering contributions in UO_2, $f(Bu)$ accounts for the effect of fission products in the crystal matrix, $g(Bu)$ accounts for irradiation defects, $h(T)$ corresponds to the temperature dependence of annealing irradiation defects, and $\frac{E}{T^2} e^{-F/T}$ accounts for polaron contributions to thermal conductivity at high temperatures. Values for these coefficients and functions are given in (Ref. 9), except for A and B, which are derived in Eq. (3).

Substituting the two coefficients for phonon scattering in 95% TD NpO_2 $A = 0.09593, B = 1.825 \times 10^{-4}$ into Eq.4 gives the expression for thermal conductivity in NpO_2 as a function of burnup and temperature. Equation (2) can then be modified to convert thermal conductivity in 95% TD NpO_2 to thermal conductivity for the fabricated density:

$$k(T)_d = k(T)_{95} \left(\frac{1-p}{1+0.5p}\right)\left(\frac{1+0.5*0.05}{1-0.05}\right) \quad (5)$$

Fig. 5 shows the thermal conductivity of NpO_2 in comparison to UO_2, both adjusted to 96% TD. The effect of 10 MWd/kg burnup on both materials is also included, as well as the measured values of Nishi (Ref. 7). The thermal conductivity is assumed constant at temperatures beyond 2400 K.

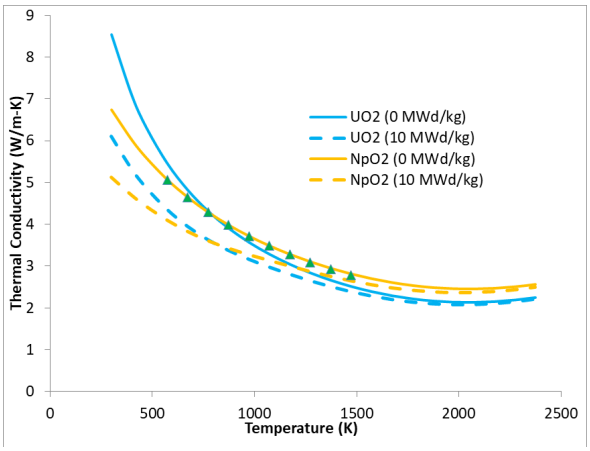

Fig. 5. Thermal conductivity of UO_2 and NpO_2. Measured values for NpO_2 from Nishi are also included.

II.D Finite Element Analysis and Results

The solution method in ANSYS is described in previous work (Ref. 10). The finite element model is developed by importing the solid model from Creo directly into SpaceClaim, which is used to simplify and parameterize the solid model. Simplifications include (1) removing all fillets and rounds and (2) reducing the capsule and cladding end caps to simpler shapes. These changes significantly improve the mesh without losing accuracy in the solution. The model is also reduced by using 180° symmetry. The final meshed model has approximately 80k elements and 380k nodes. The nominal element size is 1.1 mm in general but 0.4 mm – 0.8 mm in the pellet.

Heat generation within a pellet is dominated by the buildup of fissile isotopes. As described in Section II.B in more detail, this buildup is spatially non-uniform, which has a profound effect on the distribution of heat within the pellet. A biased mesh is imposed on the pellet to account for this non-uniformity, with a fine mesh size on the outer surface and larger elements towards the center. Fig. 6 shows the applied mesh and heat generation rate within a single pellet.

Fig. 7 shows the maximum pellet temperature profile at the end of cycle (EOC) 3 under nominal conditions. The pellet temperature is approaching the melting point at this point of irradiation due to the buildup of fissile material. The temperature bias towards the front side of the pellet (i.e., the side facing the HFIR core) is clear, with the peak temperature occurring well forward of the centerline.

II.E. Irradiation

Four Phase I capsules were fabricated and irradiated in 2018. One of the capsules was irradiated for 2 cycles, two capsules were irradiated for 3 cycles, and the final capsule was irradiated for 4 cycles. All four capsules have completed their irradiation period and are now cooling.

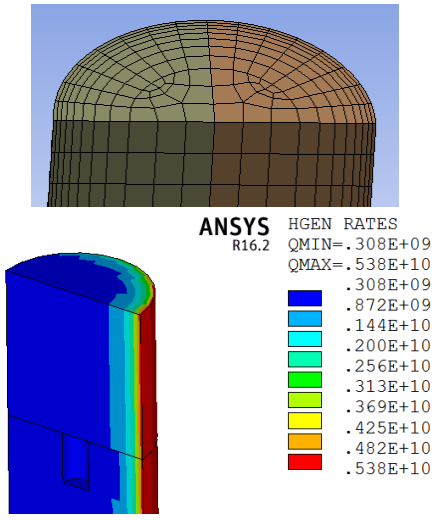

Fig. 6. Applied pellet mesh (top) and heat generation (W/m^3) at the end of cycle 3 (bottom)

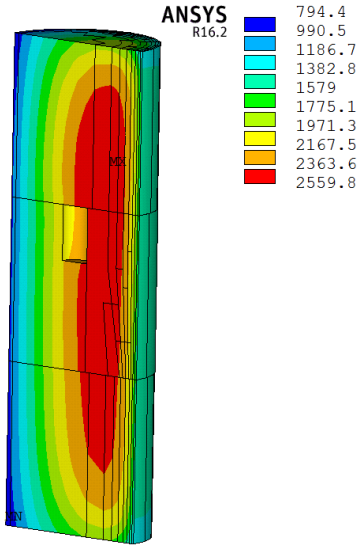

Fig. 7. Pellet temperature profile (°C) at EOC 3

The capsules will be shipped to ORNL hot cells for disassembly and post-irradiation examination in early 2019.

One of the two 3-cycle capsules will be routed to the Radiochemical Engineering Development Center for dissolution and recovery of ^{238}Pu to ascertain quality and production characteristics. The remaining three capsules will be examined for fission gas release, microstructure, and evidence of melting.

III. PHASE II MODIFICATIONS AND PRELIMINARY DESIGN

The high Phase I estimated temperatures led the design team towards several significant changes to the target design.

III.A Basket Rotation and Translation

The Phase I safety basis emphasized the detrimental effect that a static system has on heat generation due to the overexposure of the front face to the incoming neutron flux from the HFIR core. As a result, the design team requested permission from HFIR management for operators to manually rotate the target between cycles. This action reduces the buildup of fissile isotopes, spreads those isotopes over a much larger volume, and reduces fission events by placing fissile isotopes in lower flux regions. In addition, the design team compared several possible options for moving the basket from the inner small VXF to the outer small VXF to reduce the flux after the initial buildup.

III.B Elimination of Double Containment

The Phase I doubly contained design was put in place to mitigate the uncertainty associated with irradiated NpO_2 thermophysical properties and swelling/shrinking

behavior. However, this feature also introduced a second gas gap, which greatly increased the pellet temperature. Eliminating this "safety" feature improves safety by increasing margins.

III.C Smaller Pellet

The Phase I design used a pellet diameter consistent with commercial UO_2 fuel so that commercially available Zircaloy tubing could be used for the targets. However, a smaller pellet size reduces temperatures, which improves safety margins and makes the pellet easier to dissolve.

III.D Preliminary Results

The Phase II design is still ongoing, but some preliminary results are shown in Fig. 8. In the case shown in Fig. 8, a 23% smaller pellet is placed in the inner SVXF position for two cycles, with 180° rotation between cycles. The entire basket is then moved to an outer SVXF position where it receives an additional two cycles of irradiation.

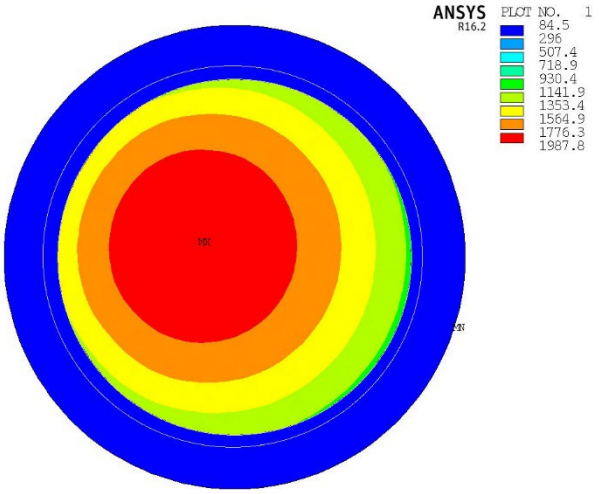

Fig. 8. Preliminary Phase II temperature profile

The Phase II modifications led to a significant reduction in temperature, albeit at the cost of a more complicated management scheme. The Phase II capsules should be easier to qualify and process.

IV. CONCLUSIONS

Using a pure NpO_2 pellet to produce ^{238}Pu has the potential to both improve production and reduce the waste stream associated with harvesting the ^{238}Pu from irradiated targets. However, the low thermal conductivity of NpO_2 and high heat generation make the target qualification difficult. This work summarizes ongoing efforts to design and qualify a pure NpO_2 target for irradiation in both HFIR and, eventually, ATR.

The Phase I target design was successfully irradiated in 2018 and is awaiting post-irradiation examination. However, the design qualification showed extremely high temperatures and low margin-to-melt due to the highly non-uniform heat generation profile within the pellet. Several design modifications being instituted in the Phase II design incorporate lessons learned from the Phase I process and have the potential to improve production and reduce pellet temperature. These modifications include using a smaller pellet, rotating the basket between cycles, and making use of the outer SVXF positions in the later cycles.

ACKNOWLEDGMENTS

The authors wish to acknowledge Chris Petrie and Prashant Jain for serving as technical reviewers of this work and Chris Bryan and Mike Crowell for providing oversight and guidance from HFIR management.

This research used resources at the High Flux Isotope Reactor, a DOE Office of Science User Facility operated by Oak Ridge National Laboratory.

REFERENCES

1. J. M. MAHATHY, *An Evaluation of Neptunium Operations at Savannah River Site*. 2016, Oak Ridge Associated Universities: Oak Ridge, TN.
2. N. XOUBI and R.T.P. III, *Modelling of the High Flux Isotope Reactor Cycle 400*. 2004: Oak Ridge National Laboratory.
3. X TEAM and X.-M.C., *MCNP - A General Monte Carlo N-Particle Transport Code, Version 5*, L.A.N. Laboratory, Editor. April 2003.
4. S. M. MOSHER, et al., *ADVANTG—An Automated Variance Reduction Parameter Generator*, O.R.N. Laboratory, Editor. 2014.
5. Haeck, W., *VESTA User's Manual - Version 2.0.0* 2009.
6. A. C. KAHLER, et al., *ENDF/B-VII.1 Neutron Cross Section Data Testing with Critical Assembly Benchmarks and Reactor Experiments.* Nuclear Data Sheets, 2011. **112**(12): p. 2997-3036.
7. T. NISHI, et al., *Thermal conductivities of minor actinide oxides for advanced fuel*, in *ATALANTE 2008*. 2008: Montpellier, France.
8. P. G. LUCUTA, H. MATZKE, and I. J. HASTINGS, *A pragmatic approach to modelling thermal conductivity of irradiated UO2 fuel: Review and recommendations.* Journal of Nuclear Materials, 1996. **232**(2-3): p. 166-180.
9. D. D. LANNING, C. E. BEYER, and K. J. GEELHOOD, *FRAPCON-3 Updates, Including Mixed-Oxide Fuel Properties* 2005, Pacific Northwest National Laboratory: Richland, WA.
10. J. L. MCDUFFEE, *Heat Transfer Through Small Moveable Gas Gaps in a Multi-body System Using the ANSYS Finite Element Software*, in *ASME 2013 Summer Heat Transfer Conference*. 2013: Minneapolis, MN, USA.